Matrix-Isolated Diglycolic Anhydride: Vibrational Spectra and Photochemical Reactivity

S. Jarmelo,*,† I. D. Reva,† L. Lapinski,‡ M. J. Nowak,‡ and R. Fausto†

Department of Chemistry, University of Coimbra, 3004-535 Coimbra, Portugal, and Institute of Physics, Polish Academy of Sciences, Al. Lotnikow 32/46, 02-668 Warsaw, Poland

Received: June 25, 2008; Revised Manuscript Received: August 11, 2008

The structure of diglycolic anhydride (1,4-dioxane-2,6-dione; DGAn) isolated in a low-temperature argon matrix at 10 K was studied by means of FTIR spectroscopy. Interpretation of the experimental vibrational spectrum was assisted by theoretical calculations at the DFT(B3LYP)/aug-cc-pVTZ level. The optimized structure of the isolated DGAn molecule adopts an envelope conformation, which was found to resemble closely the structure of DGAn in a crystal. The UV-induced ($\lambda > 240$ nm) photolysis of the matrix-isolated compound was also investigated. In order to identify the main species resulting from irradiation of the monomeric DGAn, a comparison between the DFT(B3LYP)/aug-cc-pVTZ calculated spectra of the putative products and the experimental data was carried out. The observed photoproducts can be explained by a model involving four channels: (a) 1,3-dioxolan-4-one + CO; (b) CO_2 + CO + oxirane; (c) formaldehyde + ketene + CO_2; (d) oxiran-2-one + oxiran-2-one. As a whole, the experiments indicated that the C−O−C bridge, connecting the two C═O groups, is the most reactive fragment in the molecule excited with UV light. This observation was confirmed by the natural bond orbital (NBO) analysis revealing that the most important NBO interactions are those between the carbonyl groups and the adjacent C−O and C−C bonds.

Introduction

Glycolic acid (GA) is the simplest of the α-hydroxy carboxylic acids. This compound has been the subject of numerous investigations due to its important role in essential biological processes (e.g., the photorespiratory carbon oxidation cycle in higher plants and algae or the oxalate metabolism in human beings)[1] and industrial uses, in particular in the dermatology and cosmetics industry.[2] GA has also been used as a prototype molecule for a large family of organic acids that have recently been discussed in terms of their connection to both atmospheric chemistry and spectroscopy,[3,4] and it was found in the organic content of aerosols in a polluted troposphere.[3]

GA has been recently studied in our laboratory at the monomeric level.[5] Because it has dual chemical functionality, with both alcohol (−OH) and acid (−COOH) functional groups on a very small molecule, GA possesses unique chemical attributes, as well as typical alcohol and acid chemistry. It is a useful intermediate for organic synthesis, in a range of reactions including redox,[6] esterification,[7] and long chain polymerization.[8,9]

Polyglycolic acid (PGA) is a biodegradable thermoplastic polymer and the simplest linear aliphatic polyester. It can be prepared starting from GA by means of polycondensation[9] or ring-opening polymerization.[8] In the first half of the last century, research on materials synthesized from GA was abandoned because the resulting polymers were too unstable for long-term industrial uses.[10] However, this instability, leading to biodegradation, has proven to be extremely important in medical applications. Polymers prepared from GA have found a multitude of uses in the medical industry, beginning with the biodegradable sutures first approved in the 1960s.[10] Since that time, diverse products based on GA have been accepted for use in medicine.

Oligomers of glycolic acid can be seen as precursors for polymers as well as their decomposition intermediates. One of the simplest oligomers of GA is diglycolic acid (DGAc; HOOC-CH_2-O-CH_2-COOH). The thermally induced reactivity of DGAc was recently investigated by Vinciguerra et al.[11] They found that in the 200−250 °C range DGAc undergoes simple fragmentation, forming the corresponding anhydride, with loss of a water molecule. On the other hand, diglycolic anhydride (1,4-dioxane-2,6-dione; DGAn), having the six-membered cyclic structure, is thermally more stable than DGAc and evaporates at nearly the same temperatures without degradation.

It was found that the general photoreaction pathways of cyclic anhydrides in the vapor[12] and liquid[13] phases concern decarbonylation and decarboxylation. However, diglycolic anhydride has not been studied from this viewpoint, neither experimentally nor theoretically.

In the current work, the infrared spectrum of DGAn isolated in an argon matrix at 10 K was studied in the 4000−400 cm^{-1} region. In addition, the UV-induced photochemistry of the matrix-isolated DGAn was also investigated. The assignment of the experimental vibrational spectra was assisted by calculations of the IR spectra of DGAn and of the putative photoproducts of its phototransformations. To the best of our knowledge, this is the first report on these subjects.

Experimental and Computational Methods

Diglycolic anhydride (1,4-dioxane-2,6-dione; purity ≥ 90%) was purchased from Sigma-Aldrich. Prior to the matrix-isolation experiment, a glass tube with solid DGAn was connected to the vacuum chamber of the cryostat and evacuated by pumping for 1 h. This allowed an additional purification of the compound by removing volatile impurities.

Matrixes were prepared by deposition of DGAn vapor onto a cold CsI window (10 K) directly attached to the cold tip of a continuous flow liquid helium cryostat. The vapor of the compound was deposited from a glass tube at room temperature

* Corresponding author. E-mail: sjarmelo@qui.uc.pt.
† University of Coimbra.
‡ Polish Academy of Sciences.

10.1021/jp805603b CCC: $40.75 © 2008 American Chemical Society
Published on Web 10/14/2008

TABLE 1: DFT(B3LYP)/aug-cc-pVTZ Calculated and Experimental Structural Parameters of Diglycolic Anhydride (DGAn)[a]

bond length, Å			bond angle, deg			dihedral angle, deg			
								exptl[20]	
	calcd	exptl[20]		calcd	exptl[20]		calcd	A[b]	B[b]
C_1-C_2	1.515	1.491	$C_1-C_2-O_3$	116.3	116.9	$O_7=C_2-O_3-C_4$	−171.9	−165.0	−163.7
C_4-C_5	1.515	1.493	$C_5-C_4-O_3$	116.3	116.7	$O_8=C_4-O_3-C_2$	171.9	163.1	164.5
C_2-O_3	1.386	1.379	$C_1-C_2=O_7$	124.6	125.8	$O_7=C_2-C_1-O_6$	−156.7	−157.2	−160.1
C_4-O_3	1.386	1.386	$C_5-C_4=O_8$	124.6	126.0	$O_8=C_4-C_5-O_6$	156.7	160.5	158.0
C_1-O_6	1.410	1.413	$C_2-C_1-O_6$	112.9	111.9	$O_7=C_2-C_1-H_{10}$	−37.4		
C_5-O_6	1.410	1.409	$C_4-C_5-O_6$	112.9	112.0	$O_8=C_4-C_5-H_9$	37.4		
$C_2=O_7$	1.190	1.187	$H_{10}-C_1-C_2$	108.1	107.8	$O_7=C_2-C_1-H_{12}$	79.6		
$C_4=O_8$	1.190	1.185	$H_9-C_5-C_4$	108.1	107.4	$O_8=C_4-C_5-H_{11}$	−79.6		
C_1-H_{10}	1.086	0.95	$H_{12}-C_1-C_2$	107.9	107.0	$C_2-O_3-C_4-C_5$	−7.2	−16.5	−15.0
C_5-H_9	1.086	0.94	$H_{11}-C_5-C_4$	107.9	106.6	$C_4-O_3-C_2-C_1$	7.2	14.9	16.4
C_1-H_{12}	1.099	0.98	$H_{10}-C_1-O_6$	107.9	109.1	$C_2-C_1-O_6-C_5$	−56.0	−59.3	−57.3
C_5-H_{11}	1.099	0.97	$H_9-C_5-O_6$	107.9	108.4	$C_4-C_5-O_6-C_1$	56.0	57.3	58.7
			$H_{12}-C_1-O_6$	111.6	111.0	$O_3-C_2-C_1-O_6$	24.3	23.0	19.8
			$H_{11}-C_5-O_6$	111.6	111.6	$O_3-C_4-C_5-O_6$	−24.3	−20.0	−22.5
			$C_2-O_3-C_4$	123.2	121.2	$O_3-C_2-C_1-H_{10}$	143.6		
			$C_1-O_6-C_5$	111.9	110.7	$O_3-C_4-C_5-H_9$	−143.6		
						$O_3-C_2-C_1-H_{12}$	−99.5		
						$O_3-C_4-C_5-H_{11}$	99.5		

[a] See Figure 1 for atom numbering. [b] The crystal unit cell consists of two independent DGAn molecules (referred to in the original work as A and B). The bond lengths and valence angles for these two molecules were found to be equal within the estimated standard deviation and thus were averaged, while the dihedral angles were found to be slightly different (see ref 20).

(24 °C), together with a large excess of the matrix gas (argon). Argon of spectral purity (6.0) was supplied by Linde AG. The infrared spectra were recorded in the range 4000−400 cm^{-1}, with 0.5 cm^{-1} resolution, using a Thermo Nicolet Nexus 670 FTIR spectrometer, equipped with a KBr beamsplitter. The matrix was irradiated through the outer quartz window of the cryostat with light from an HBO200 high-pressure mercury lamp. This lamp was fitted with a water filter (to remove IR radiation) and a suitable cutoff filter, UG11 or UG5 (Schott), transmitting light with $\lambda > 270$ nm or $\lambda > 240$ nm, respectively.

Theoretical calculations were performed using the Gaussian 03 program package[14] at the DFT(B3LYP) level of theory,[15] with the Dunning aug-cc-pVTZ basis set.[16] At the optimized geometries of the investigated molecules (Table 1), the harmonic vibrational frequencies and IR intensities were calculated. To correct for the systematic shortcomings of the applied methodology (mainly for anharmonicity), the predicted vibrational wavenumbers were scaled down by a single factor of 0.99. The theoretical normal modes were analyzed by carrying out the potential energy distribution (PED) calculations. Transformations of the force constants with respect to the Cartesian coordinates to the force constants with respect to the molecule fixed internal coordinates allowed the PED analysis to be carried out as described by Schachtschneider and Mortimer.[17] The internal symmetry coordinates used in the analysis of the normal modes of the DGAn molecule are listed in Table 2. The elements of the computed PED matrixes greater than 10% are presented in Table 3.

To better understand the specific nature of the intramolecular interactions, the electronic structure of DGAn was characterized by natural bond orbital (NBO) analysis, using NBO version 3, as implemented in Gaussian 03.[14]

Results and Discussion

Theoretical Calculations of the Structure of Diglycolic Anhydride. The DGAn molecule would adopt the structure with the highest possible symmetry (C_{2v}) if all the carbon and oxygen atoms were located in the same plane (and the methylene hydrogen atoms situated symmetrically with respect to this plane). For a six-membered ring, this would imply that the angles formed by heavy atoms would be approximately equal to 120°. However, the ring angles around the saturated carbon atoms of the two methylene groups tend to be approximately tetrahedral, i.e., ≈ 109.47°. Then, a more energetically favorable structure would be adopted if the angle strain in the six-membered ring could be reduced by changing the molecular geometry without implying large changes in the a priori preferred angles around the ring atoms. To satisfy this requirement, the molecule must depart from the C_{2v} symmetry. Indeed, taking into consideration the above reasoning, Le Fèvre and Sundaram,[18] in an early attempt to characterize the equilibrium geometry of DGAn molecule, predicted it to adopt a 'chair' structure, where both ring oxygen atoms would not share the plane of the four carbon atoms.

In the present study, the geometry of the DGAn molecule was optimized under C_{2v}, C_2, C_s, and C_1 symmetry constraints at the DFT(B3LYP)/6-311++G(d,p) level of theory. The C_{2v} and C_2 structures were found to be second- and first-order transition states, respectively. The C_s structure was characterized as a true minimum, while optimization without symmetry restrictions (C_1 point group) converged to a geometry closely resembling the C_s structure. The calculations carried out at the MP2/6-311++G(d,p) level were essentially in agreement with the DFT results.

The geometry optimizations were then repeated at the higher theory level, DFT(B3LYP)/aug-cc-pVTZ. These calculations also yield a single minimum on the ground-state potential energy surface of the molecule, corresponding to the C_s structure (see Figure 1) This was confirmed by the vibrational analysis which did not show any imaginary frequencies for the C_s structure.[19] Interestingly, the minimum-energy structure found in our calculations is different from that suggested in the work of Le Fèvre and Sundaram.[18] The DFT(B3LYP)/aug-cc-pVTZ calculations, carried out in the current work, predict only one ring oxygen atom to depart substantially from the plane of the remaining heavy atoms (see Figure 1).

The geometrical parameters calculated for DGAn in the present study are collected in Table 1 and compared there with

TABLE 2: Internal Symmetry Coordinates Used in the Normal Mode Analysis for Diglycolic Anhydride[a]

$S_1 = 2^{-1/2}\,(r_{1,6} + r_{5,6})$	$\nu_s(CO)'$
$S_2 = 2^{-1/2}\,(r_{1,6} - r_{5,6})$	$\nu_a(CO)'$
$S_3 = 2^{-1/2}\,(r_{1,2} + r_{5,4})$	$\nu_s(CC)$
$S_4 = 2^{-1/2}\,(r_{1,2} - r_{5,4})$	$\nu_a(CC)$
$S_5 = 2^{-1/2}\,(r_{2,3} + r_{4,3})$	$\nu_s(CO)''$
$S_6 = 2^{-1/2}\,(r_{2,3} - r_{4,3})$	$\nu_a(CO)''$
$S_7 = 2^{-1/2}\,(r_{2,7} + r_{4,8})$	$\nu_s(C{=}O)$
$S_8 = 2^{-1/2}\,(r_{2,7} - r_{4,8})$	$\nu_a(C{=}O)$
$S_9 = 2^{-1/2}\,(r_{1,10} + r_{5,9})$	$\nu_s(CH)'$
$S_{10} = 2^{-1/2}\,(r_{1,10} - r_{5,9})$	$\nu_a(CH)'$
$S_{11} = 2^{-1/2}\,(r_{1,12} + r_{5,11})$	$\nu_s(CH)''$
$S_{12} = 2^{-1/2}\,(r_{1,12} - r_{5,11})$	$\nu_a(CH)''$
$S_{13} = 6^{-1/2}\,(\beta_{6,2,1} - \beta_{1,3,2} + \beta_{2,4,3} - \beta_{3,5,4} + \beta_{4,6,5} - \beta_{5,1,6})$	β(R1)
$S_{14} = 12^{-1/2}\,(2\beta_{2,4,3} - \beta_{3,5,4} - \beta_{4,6,5} + 2\beta_{5,1,6} - \beta_{6,2,1} - \beta_{1,3,2})$	β(R2)
$S_{15} = 1/2\,(\beta_{6,2,1} - \beta_{1,3,2} + \beta_{3,5,4} - \beta_{4,6,4})$	β(R3)
$S_{16} = 1/2\,(\beta_{3,7,2} - \beta_{1,7,2} + \beta_{3,8,4} - \beta_{5,8,4})$	$\beta_s(C{=}O)$
$S_{17} = 1/2\,(\beta_{3,7,2} - \beta_{1,7,2} - \beta_{3,8,4} + \beta_{5,8,4})$	$\beta_a(C{=}O)$
$S_{18} = 2^{-1/2}\,(\beta_{10,12,1} + \beta_{9,11,5})$	$\mathrm{scis_s(CH_2)}$
$S_{19} = 2^{-1/2}\,(\beta_{10,12,1} - \beta_{9,11,5})$	$\mathrm{scis_a(CH_2)}$
$S_{20} = 8^{-1/2}\,(\beta_{6,10,1} - \beta_{6,12,1} + \beta_{2,10,1} - \beta_{2,12,1} + \beta_{6,9,5} - \beta_{6,11,5} + \beta_{4,9,5} - \beta_{4,11,5})$	$\mathrm{rock_s(CH_2)}$
$S_{21} = 8^{-1/2}\,(\beta_{6,10,1} - \beta_{6,12,1} + \beta_{2,10,1} - \beta_{2,12,} - \beta_{6,9,5} + \beta_{6,11,5} - \beta_{4,9,5} + \beta_{4,11,5})$	$\mathrm{rock_a(CH_2)}$
$S_{22} = 8^{-1/2}\,(\beta_{6,10,1} + \beta_{6,12,1} - \beta_{2,10,1} - \beta_{2,12,1} + \beta_{6,9,5} + \beta_{6,11,5} - \beta_{4,9,5} - \beta_{4,11,5})$	$\mathrm{wag_s(CH_2)}$
$S_{23} = 8^{-1/2}\,(\beta_{6,10,1} + \beta_{6,12,1} - \beta_{2,10,1} - \beta_{2,12,1} - \beta_{6,9,5} - \beta_{6,11,5} + \beta_{4,9,5} + \beta_{4,11,5})$	$\mathrm{wag_a(CH_2)}$
$S_{24} = 8^{-1/2}\,(\beta_{6,10,1} - \beta_{6,12,1} - \beta_{2,10,1} + \beta_{2,12,1} + \beta_{6,9,5} - \beta_{6,11,5} - \beta_{4,9,5} + \beta_{4,11,5})$	$\mathrm{twist_s(CH_2)}$
$S_{25} = 8^{-1/2}\,(\beta_{6,10,1} - \beta_{6,12,1} - \beta_{2,10,1} + \beta_{2,12,1} - \beta_{6,9,5} + \beta_{6,11,5} + \beta_{4,9,5} - \beta_{4,11,5})$	$\mathrm{twist_a(CH_2)}$
$S_{26} = 2^{-1/2}\,(\gamma_{8,5,4,3} + \gamma_{7,3,2,1})$	$\gamma_s(C{=}O)$
$S_{27} = 2^{-1/2}\,(\gamma_{8,5,4,3} - \gamma_{7,3,2,1})$	$\gamma_a(C{=}O)$
$S_{28} = 6^{-1/2}\,(\tau_{4,3,2,1} - \tau_{3,2,1,6} + \tau_{2,1,6,5} - \tau_{1,6,5,4} + \tau_{6,5,4,3} - \tau_{5,4,3,2})$	τ(R1)
$S_{29} = 1/2\,(\tau_{4,3,2,1} - \tau_{2,1,6,5} + \tau_{1,6,5,4} - \tau_{5,4,3,2})$	τ(R2)
$S_{30} = 12^{-1/2}\,(2\tau_{3,2,1,6} - \tau_{4,3,2,1} - \tau_{2,1,6,5} + 2\tau_{6,5,4,3} - \tau_{1,6,5,4} - \tau_{5,4,3,2})$	τ(R3)

[a] See Figure 1 for atom numbering. $r_{m,n}$ is the distance between atoms A_m and A_n; $\beta_{m,n,l}$ is the angle between vectors A_lA_m and A_lA_n; $\gamma_{m,n,l,o}$ is the angle between the vector A_lA_m and the plane defined by atoms A_n, A_l, A_o; $\tau_{m,n,l,o}$ is the dihedral angle between the plane defined by A_m, A_n, A_l and the plane defined by A_n, A_l, A_o atoms; s = symmetric; a = antisymmetric; ν = stretching; β = in-plane bending; γ = out-of-plane bending; τ = torsion; scis = scissoring; rock = rocking; wag = wagging; twist = twisting.

the experimental values obtained for DGAn in crystals.[20] Since the molecule of DGAn is fairly rigid and free of hydrogen bonds in the solid state, the geometry in the crystal is expected to undergo only small distortions compared to the free molecule. Indeed, the similarity between the crystal data and those calculated for the monomer in vacuum is notable (see Table 1).

In the crystal, similarly as for the isolated molecule, the four carbon atoms are essentially planar (deviations from planarity do not exceed 0.01 Å) and only one ring oxygen atom (O_6) deviates substantially from this plane (ca. 0.63 Å). The three remaining oxygen atoms deviate no more than 0.17 Å from the plane of carbon atoms,[20] indicating the extent of flattening of the molecule. The global shape of the molecule then resembles the envelope conformation [see an example of the envelope conformation in a six-membered ring in ref 21].

In the minimum energy configuration, the molecular symmetry plane contains the two ring oxygen atoms (O_3 and O_6) and bisects the molecule (it is perpendicular to the plane of the carbon atoms), Figure 1. The $C_2-C_1-O_6$ and $C_4-C_5-O_6$ angles are equal to 112.9° (see Table 1), indicating that the atom arrangements at C_1 and C_5 are essentially tetrahedral. The calculated value of the $C_1-O_6-C_5$ angle is equal to 111.9°, which is close to the COC unstrained angle in dimethyl ether (112.7°, calculated at the same DFT(B3LYP)/aug-cc-pVTZ level for the purpose of the present study; 111.8°, as determined by gas electron-diffraction and microwave spectroscopy).[22]

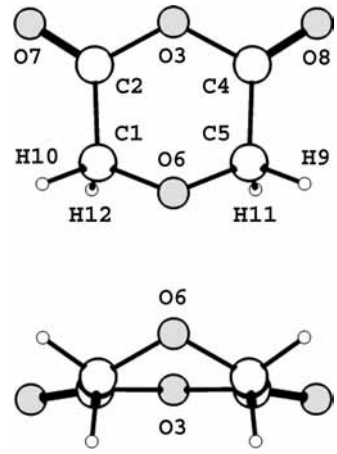

Figure 1. Optimized [DFT(B3LYP)/aug-cc-pVTZ] structure of diglycolic anhydride (DGAn) and atom numbering adopted in this study. Top: Front view. Bottom: View along the C2−O3−C4 plane. The ring atom numbering in this study was chosen to be different from the IUPAC recommendation, in order to facilitate the comparison with two related molecules previously studied, glutarimide and 5,6-dihydrouracil (DHU) (see ref 19).

Infrared Spectrum of Diglycolic Anhydride. One of the main advantages of the matrix-isolation technique is the very small change introduced to the geometry of the embedded guest molecules by the inert matrix environment. Hence, the structure of matrix-isolated molecules is essentially the same as the structure of these molecules in vacuum. Therefore, a direct comparison between the experimental matrix-isolation infrared spectra and the spectra calculated for the molecule in vacuum is an efficient tool for the structural characterization of matrix-isolated species.

The harmonic vibrational frequencies and the corresponding infrared intensities were calculated [at the DFT(B3LYP)/aug-cc-pVTZ level] for the optimized structure of DGAn (shown in Figure 1). The calculated normal modes were analyzed in terms of their potential energy distribution (PED). The definitions of the internal symmetry coordinates used in the PED analysis are provided in Table 2.

The theoretically calculated spectrum of DGAn is compared with the experimental FTIR spectrum of matrix-isolated DGAn in Figure 2 and in Table 3. The good agreement between the experimental and calculated spectra validates the theoretically calculated structure of the DGAn monomer and allows a reliable assignment of the experimental IR bands.

The most intense band (at 1800 cm^{-1}) in the IR spectrum of DGAn is associated with the antisymmetric (A'') stretching vibration of the two C=O groups [$\nu_a(C{=}O)$], whereas the symmetric (A') stretching mode is associated with the matrix-site-split band with maxima at 1841, 1838, and 1835 cm^{-1}. The relatively intense band at ca. 1785 cm^{-1} belongs also to the spectrum of DGA monomers. This band is assigned to the $\nu_s(CO)' + \beta_a(C{=}O)$ combination tone (A'') enhanced through Fermi resonance with $\nu_a(C{=}O)$. The $\nu_s(CO)'$ and $\beta_a(C{=}O)$ fundamentals are observed at 1250 and 539 cm^{-1}, respectively (see Table 3).

TABLE 3: Observed (Argon Matrix) and DFT(B3LYP)/aug-cc-pVTZ Calculated IR Spectrum for Diglycolic Anhydride (DGAn): Frequencies (freq, cm^{-1}), Potential Energy Distribution of the Normal Modes (PED, %), and Absolute Intensities (int, km mol^{-1}) of the Corresponding IR Bands

experimental Ar matrix		calculated DFT(B3LYP)/aug-cc-pVTZ			
freq	int[a]	freq[b]	int	symm	PED[c]
n.o.[f]	n.o.[f]	3101.4	<1	A'	**ν_s(CH)′ (98)**[d]
		3100.0	3	A''	**ν_a(CH)′ (98)**
2892, 2845	vw, vw	2945.2	30	A'	**ν_s(CH)″ (99)**
		2944.6	13	A''	**ν_a(CH)″ (98)**
1841, 1838, 1835	s, m, m	1860.5	135	A'	**ν_s(C═O) (91)**
1800[e]	vs	1818.6	520	A''	**ν_a(C═O) (93)**
1440, 1437, 1436	sh, sh, w	1460.7	18	A'	**scis$_s$(CH_2) (99)**
1428	vw	1452.5	1	A''	**scis$_a$(CH_2) (100)**
1364	vw	1377.1	2	A'	**wag$_s$(CH_2) (90)**
1332, 1330	sh, m	1341.5	17	A''	**wag$_a$(CH_2) (96)**
1288, 1280	vw, br	1295.4	5	A'	**twist$_s$(CH_2) (88)**
1238, 1236	sh, vs	1245.3	113	A''	**twist$_a$(CH_2) (81)**, ν_a(CO)′ (10)
1254, 1250	sh, s	1239.7	85	A'	**ν_s(CO)″ (29)**, β_s(C═O) (28), ν_s(CC) (28)
1173, 1167	vw, vs	1164.6	312	A''	**ν_a(CO)′ (66)**, twist$_a$(CH_2) (28), ν_a(CC) (11)
1090	vs	1080.0	223	A''	**ν_a(CO)″ (33)**, rock$_a$(CH_2) (17), ν_a(CC) (16), ν_a(CO)′ (14), β(R3) (12)
1043	w	1046.4	7	A'	**rock$_s$(CH_2) (62)**, γ_s(C═O) (16)
979	m	993.9	18	A''	**rock$_a$(CH_2) (62)**, γ_a(C═O) (23)
		972.3	32	A'	**ν_s(CO)′ (85)**
937	s	933.5	85	A''	ν_a(CO)″ (45), **ν_a(CC) (32)**, β_a(C═O) (20)
824, 820	m, m	818.8	39	A'	**β(R1) (50)**, ν_s(CC) (19), γ_s(C═O) (11)
661	vw	656.2	7	A'	**ν_s(CC) (38)**, ν_s(CO)″ (23), β(R1) (13), γ_s(C═O) (12)
600	m	603.0	24	A''	**γ_a(C═O) (55)**, β(R3) (17), rock$_a$(CH_2) (14)
540, 539	sh, s	538.6	37	A''	**β_a(C═O) (64)**, ν_a(CC) (24)
		536.5	8	A'	**γ_s(C═O) (51)**, rock$_s$(CH_2) (18), β(R1) (14)
458	vw	458.3	4	A''	**β(R3) (63)**, ν_a(C═O) (14)
n.i.[f]	n.i.[f]	449.9	0.2	A'	**β(R2) (40)**, ν_s(CO)″ (20), γ_s(C═O) (18)
n.i.[f]	n.i.[f]	369.0	18	A'	β_s(C═O) (47), β(R2) (38)
n.i.[f]	n.i.[f]	273.3	17	A'	**τ(R2) (56)**, τ(R1) (38)
n.i.[f]	n.i.[f]	122.9	3	A'	**τ(R1) (53)**, τ(R2) (48)
n.i.[f]	n.i.[f]	73.0	1	A''	**τ(R3) (101)**

[a] Qualtitative intensities: vs, very strong; s, strong; m, medium; w, weak; vw, very weak; br, broad; sh, shoulder. [b] DFT harmonic frequencies were scaled using a single scaling factor of 0.99. [c] s = symmetric; a = antisymmetric; ν = stretching; β = in-plane bending; γ = out-of-plane bending; τ = torsion; scis = scissoring; rock = rocking; wag = wagging; twist = twisting. See Table 2 for the definition of the symmetry coordinates used in the normal-mode analysis for DGAn (atom numbering as in Figure 1). PEDs lower than 10% not included. [d] Normal modes in bold font are the approximate description. [e] The strong band at 1784 cm^{-1} and the two shoulders at higher wavenumbers, 1788 and 1786 cm^{-1}, are due to a Fermi resonance interaction involving the combination tone ν_s(CO)′ + β_a(C═O). [f] n.o. = not observed; n.i. = not investigated.

In the 1850−1500 cm^{-1} spectral region only the bands due to the two carbonyl stretching modes are predicted by the theoretical calculations. Accordingly, in the experimental spectrum of monomeric DGAn this spectral range is free of any absorptions of non-negligible intensity. In addition, the bands due to the scissoring vibrations of CH_2 groups, predicted and observed in the 1460−1430 cm^{-1} range, are of low intensity. Altogether, this creates a characteristic gap from 1800 to 1350 cm^{-1} in the IR spectrum of DGAn.

It is also worth noticing that all the intense IR bands appearing in the 1250−900 cm^{-1} range are due to modes with significant contributions from the stretching vibrations of the C−O bonds, the most intense ones corresponding to the antisymmetric stretching modes [ν_a(CO)′ and ν_a(CO)″]. In the low-frequency range (600−535 cm^{-1}), the most intense bands are of medium intensity and originate from the γ_a(C═O) and β_a(C═O) vibrations.

UV Induced Photochemistry of Diglycolic Anhydride. DGAn monomers isolated in an argon matrix were subjected to a series of UV irradiations with different long-pass filters, gradually decreasing the cutoff wavelength, and thus increasing the transmitted UV energy. No UV-induced changes were observed when the matrix was irradiated with light of λ > 270 nm. Upon irradiation with UV light of shorter wavelengths (λ > 240 nm), the IR bands due to DGAn started to decrease and new absorptions appeared in the spectrum. At this cutoff wavelength, a series of irradiations was carried out, with different exposure times. After 6 h of irradiation, ca. 52% of the reagent was consumed.

The spectrum of the photoproducts resulting from the UV irradiation of matrix-isolated DGAn is presented in Figure 3 (top frame). This spectrum was obtained by subtracting the spectrum of the initially deposited compound (scaled with the factor 0.48) from the spectrum of the sample recorded after 6 h of irradiation.

Interpretation of the bands in the 2500−1600 cm^{-1} region (Figure 3) is the key to solve the photochemistry of DGAn. This region is characteristic of CO_2, CO, and the carbonyl stretching vibrations, whose frequencies are particularly sensitive to the size of the ring to which the C═O group is attached.[23] Chart 1 shows the structures of the possible products of DGAn photochemistry (see a detailed discussion below). Whenever possible, the assignment of bands due to these photoproducts was validated by comparison with the experimental spectra of the compounds isolated in low-temperature inert matrixes or in the gas phase.

CHART 1: Structures of Reagent (Diglycolic Anhydride) and Possible Photoproducts

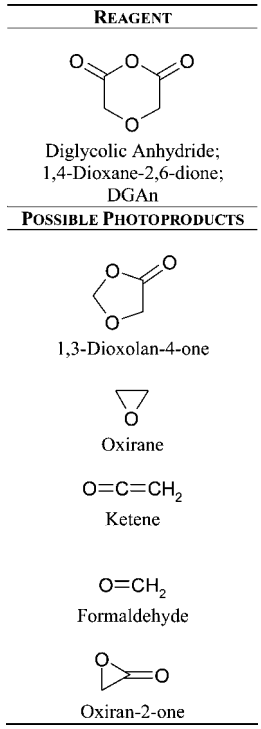

SCHEME 1: Experimentally Observed Photoproducts Formed after UV Irradiation of Matrix-Isolated Diglycolic Anhydride (DGAn) and Suggested Routes of Unimolecular Decomposition of DGAn Leading to These Photoproducts[a]

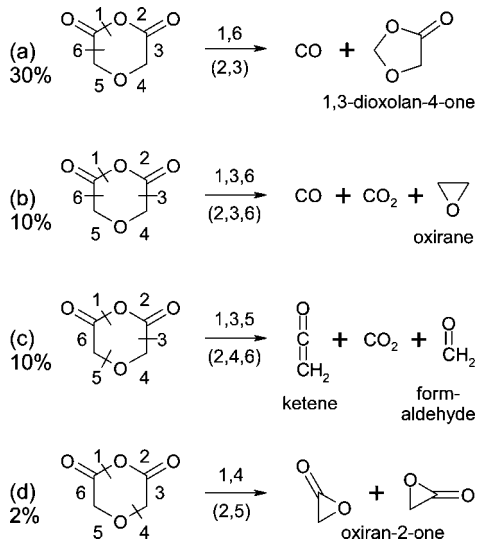

[a] Different reaction channels (a−d) are accompanied by their efficiencies in terms of the amount of the consumed reagent (the total is 52%). The ring bonds in the reagent molecule are numbered from 1 to 6. The crossed bonds are the bonds that undergo cleavage in particular photochannels; the same bonds are shown over the reaction arrows. The numbers in parentheses below the reaction arrows designate the symmetrically equivalent combinations.

The antisymmetric stretching vibration of monomeric CO_2 gives rise to the very characteristic bands between 2345 and 2339 cm^{-1}.[24]

The band due to the antisymmetric stretching vibration in the RHC=C=O species [in ketene itself (R = H)[25] and in substituted ketenes (R = alkyl group)] has a typical frequency[26] of ca. 2140−2138 cm^{-1}. However, assignment to ketene cannot be unequivocal in this spectral region, since carbon monoxide also absorbs at the same frequencies.[27]

The absorptions above 1900 cm^{-1} are characteristic of stretching vibrations of carbonyl groups attached to three-membered rings. For example, in gaseous cyclopropanone[28] the frequency of the stretching vibration of the C=O group is equal to 1906 cm^{-1}. Deltic acid[29] and its dimethyl ester,[30] produced by in situ broadband UV irradiation of the matrix-isolated squaric acid and squaric acid dimethyl ester, respectively, give rise to the IR bands appearing at 1905 cm^{-1} and in the 1950−1850 cm^{-1} region, respectively. Oxiran-2-one ring system is another good candidate for absorption at such a high frequency.[31] Isomeric open-chain structures are expected to exhibit absorptions at much lower frequencies.[32]

Absorptions in the 1850−1800 cm^{-1} spectral region are expected for carbonyl groups attached to four- or five-membered rings. For example, for gaseous cyclobutanone, the carbonyl stretching vibration was reported at 1815 cm^{-1},[28] whereas for matrix-isolated 2(5H)-furanone the carbonyl stretching band was found at 1794 cm^{-1}.[23,33,34] In the photochemistry of DGAn, a photoproduct with a carbonyl group attached to a five-membered ring can be obtained by decarbonylation of the DGAn molecule. This species (1,3-dioxolan-4-one, Chart 1) could be responsible for the absorptions at 1832.6, 1817.4, and 1814.6 cm^{-1}.

Finally, the absorption at 1740−1738 cm^{-1} is characteristic of matrix-isolated formaldehyde ($O=CH_2$).[35]

Interpretation of the experimental data was further assisted by theoretical calculations [at the DFT(B3LYP)/aug-cc-pVTZ level]. By analogy with the crystals of DGAn, where the structure of monomeric units is weakly affected by the neighboring molecules,[20] we assumed that intermolecular interactions between the products of decomposition of DGAn formed in the same argon matrix cage are also weak. In such a case, the spectra of the associates should not differ much from the spectra of the individual species. Indeed, as it was recently observed for the molecules of diazines (pyrazine, pyrimidine, and pyridazine), the spectra of the matrix-isolated monomeric species strongly resemble the spectra of the corresponding crystals.[36] Such a resemblance can be attributed to the absence of the intermolecular hydrogen bonds, which may strongly affect the vibrational spectra of the aggregates even at the dimeric level.[37] Such compounds as formaldehyde, ketene, CO, and CO_2 (that can appear as photoproducts of DGAn, see below) do not form hydrogen bonds and thus the dimers (or trimers) including these species were not simulated in the calculations. All the calculations on the photoproducts were performed for the monomers. The validity of such approach was demonstrated in our previous study,[38] where no significant difference was found between the spectra of individual photoproducts (like CO and CO_2) and the spectra of matrix-isolated complexes containing these products.

Following the above-described strategy of interpretation, we suggest a model for the observed photochemistry. The UV-induced decomposition of matrix-isolated DGAn can be explained in terms of four photochemical processes, schematically shown in Scheme 1. These photoreactions should generate seven different photoproducts: carbon dioxide, ketene, carbon monoxide, oxiran-2-one, 1,3-dioxolan-4-one, formaldehyde, and oxirane (see Chart 1 and Scheme 1). In order to assess the amounts of these species, the calculated intensities of the IR bands due to these products were reduced to match the experimentally observed data (compare top and middle frames of Figure 3). In that way, the relative efficiencies of the four

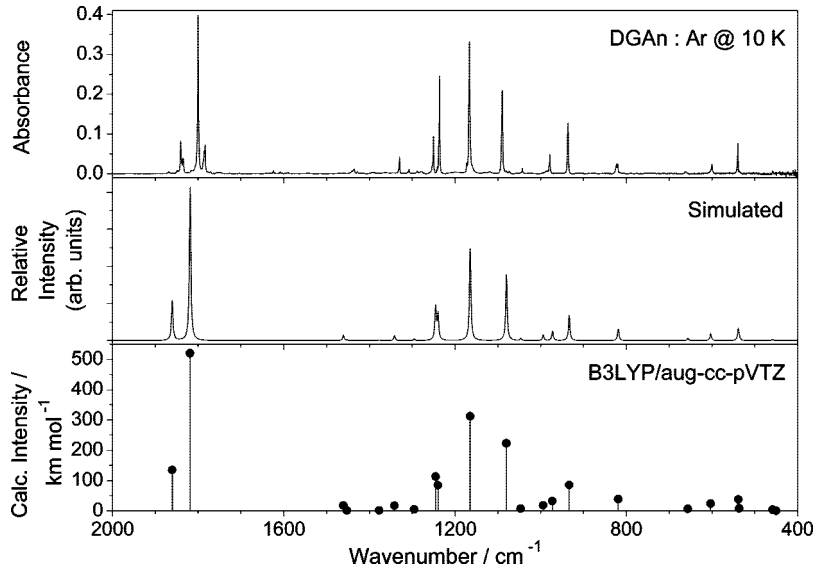

Figure 2. Top: Experimental FTIR spectrum of diglycolic anhydride (DGAn) trapped in an argon matrix at 10 K. Bottom: Infrared spectrum of a DGAn monomer in vacuum calculated at the DFT(B3LYP)/aug-cc-pVTZ level of theory in harmonic approximation. The calculated wavenumbers were scaled by a factor of 0.99 (obtained from the least-squares linear fit). Middle: Simulated spectrum created using Lorentzian functions centered at the scaled calculated wavenumbers and with bandwidths at half-height equal to 5 cm^{-1}.

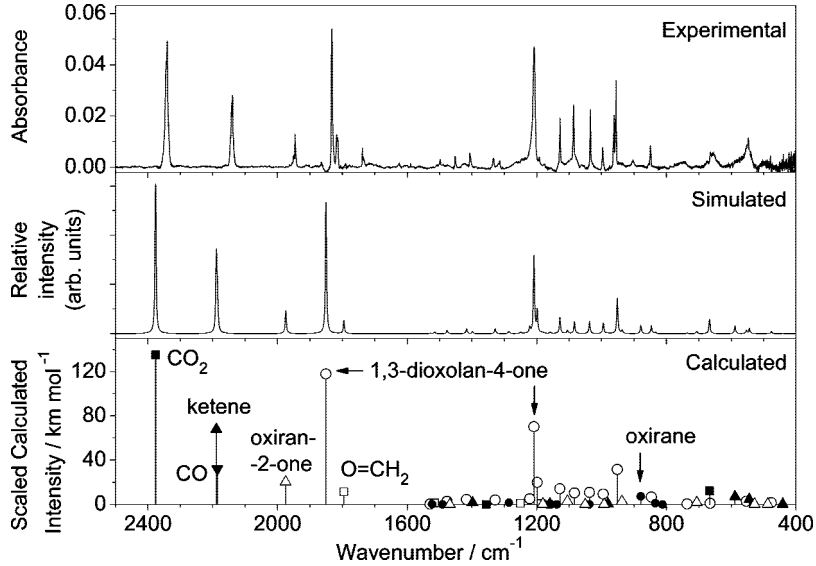

Figure 3. Top: Experimental FTIR spectrum of photoproducts emerging upon UV (λ > 240 nm) irradiation of diglycolic anhydride (DGAn) isolated in an argon matrix at 10 K. The bands due to the nonreacted starting compound were nullified. Bottom: Infrared spectra of putative photoproducts calculated at the DFT(B3LYP)/aug-cc-pVTZ level of theory in harmonic approximation. The calculated wavenumbers were scaled by a factor of 0.99. The calculated intensities of individual compounds were scaled to attain the best match between the simulated and experimental spectra (see text). Middle: Superposition spectrum of the compounds shown in the bottom frame. This spectrum was simulated using Lorentzian functions centered at the scaled calculated wavenumbers and with bandwidths at half-height equal to 5 cm^{-1}.

pathways of UV-induced decomposition of DGAn were obtained. The values of these efficiencies (shown in Scheme 1) were normalized so that their sum is equal to 52%, i.e., to the percent of DGAn consumed in the photoreactions.

More than a half of the reacted compound (30%) is consumed in channel a (Scheme 1), where DGAn undergoes decarbonylation and forms 1,3-dioxolan-4-one. The latter photoproduct is characterized by a strong absorption centered at ca. 1830 cm^{-1}.[33] 1,3-Dioxolan-4-one has a very characteristic pattern of six bands in the 1220−950 cm^{-1} region of the infrared spectrum (Figure 4). They are due to the vibrations of methylene groups [twist$_a$(CH$_2$)/rock$_a$(CH$_2$): 1208.4 cm^{-1}; twist$_s$(CH$_2$): 1128.0 cm^{-1}; wag$_a$(CH$_2$): 1086.5 cm^{-1}; and rock$_s$(CH$_2$): 1034.4 cm^{-1}] and C−O$_{ring}$ stretching (1000−950 cm^{-1}); see also Table 4. The agreement between the spectrum calculated for 1,3-dioxolan-4-one and the corresponding bands in the experimental IR spectrum of the photoproducts generated upon UV irradiation of DGAn monomers is so good (see Figure 4) that the identification of this species seems to be unquestionable.

Another 10% of the reagent, consumed in channel b, is phototransformed into CO, CO_2, and oxirane. A further 10% decomposes in channel c to give ketene, CO_2, and formaldehyde. Finally, in channel d, accounting for the remaining 2% of the reacted substrate, the DGAn molecule is transformed in two molecules of oxiran-2-one (see Scheme 1). After reducing the calculated intensities of IR bands in the spectra of photoproducts generated in channels a, b, c, and d to 30, 10, 10, and 2%, respectively, the simulated superposition spectrum of all photoproducts is in a fairly good agreement with the experiment (Figure 3).

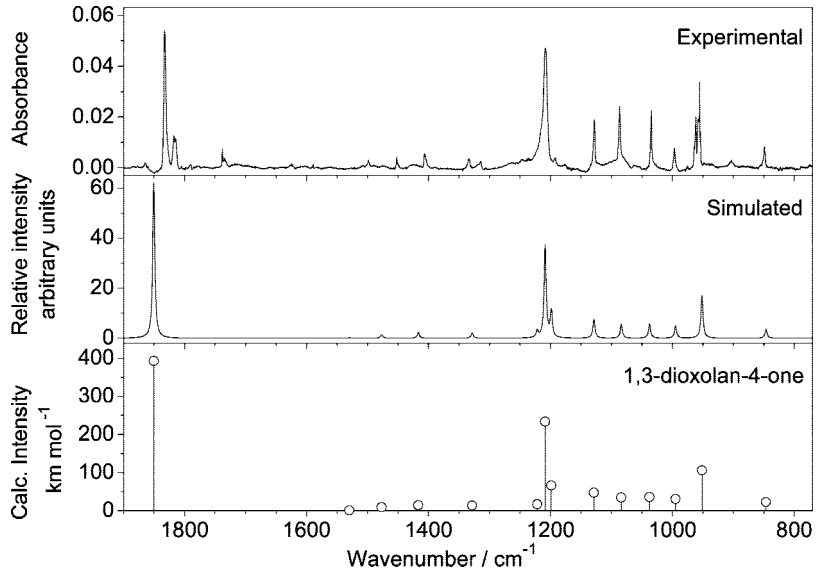

Figure 4. Top: Fragment of the experimental FTIR spectrum of photoproducts emerging upon UV ($\lambda > 240$ nm) irradiation of diglycolic anhydride (DGAn) isolated in an argon matrix at 10 K. The bands due to the nonreacted starting compound were nullified. Bottom: Infrared spectrum of 1,3-dioxolan-4-one calculated at the DFT(B3LYP)/aug-cc-pVTZ level of theory in harmonic approximation. The calculated wavenumbers were scaled by a factor of 0.99. Middle: Simulated infrared spectrum of the 1,3-dioxolan-4-one monomers obtained using Lorentzian functions centered at the scaled calculated wavenumbers and with bandwidths at half-height equal to 5 cm^{-1}.

SCHEME 2: Some Hypothetic Photochemical Transformations of Diglycolic Anhydride (DGAn)[a]

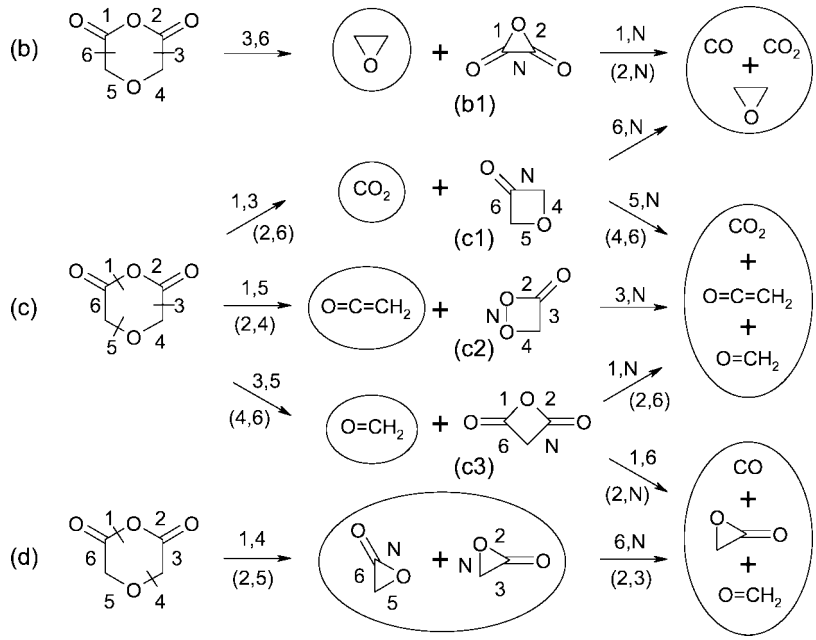

[a] The observed photoproducts are enclosed in ovals. The ring bonds in the reagent molecule are numbered from 1 to 6. The same numbers are indicated in the structures of the photoproducts. The bonds that undergo cleavage at the start of particular photochannels are crossed. The newly formed bonds are designated by "N". The pairs of bonds (numbers) over the reaction arrow designate the bonds undergoing cleavage, and the numbers in parentheses below the reaction arrows designate the symmetrically equivalent combinations. Compounds designated as b1, c1, c2, and c3 were not identified in the experiment.

The vibrational signatures of six of the seven photoproducts proposed by the model presented in Scheme 1 were already discussed above, during the assignments of the carbonyl stretching region. The seventh photoproduct, oxirane, does not contain a carbonyl fragment and should absorb at lower frequencies. The infrared spectrum of oxirane in the gas phase exhibits an intense band at 877 cm^{-1} (ref 39), and the DFT(B3LYP)/aug-cc-pVTZ calculation predicts this feature to appear at 878.8 cm^{-1}. This mode (due to the deformation of the oxirane three-membered ring) was assigned to the experimental band found at 903.3 cm^{-1} in the spectrum of the photoproducts generated from DGAn (Figure 3). The full comparison of the experimental and calculated spectra due to the DGAn photolysis products is presented in Table 4.

Mechanisms of UV-Induced Photochemistry. The six-membered ring of DGAn is saturated, i.e., all ring bonds are formally single. As a consequence, closed-shell photoproducts can be formed only if the photochemical cleavage of one of the ring bonds is accompanied by cleavage of other bond(s). From the viewpoint of photochemistry, it is instructive to compare DGAn with other cyclic molecules with several single bonds in their rings. The five-membered rings of tetrazoles and

TABLE 4: Experimental and Calculated [DFT(B3LYP)/aug-cc-pVTZ; Scaled by 0.99] Vibrational Frequencies (cm^{-1}) and Calculated Infrared Intensities (km mol^{-1}) for Carbon Dioxide, Carbon Monoxide, Ketene, Oxiran-2-one, 1,3-Dioxolan-4-one, Formaldehyde, and Oxirane[a]

		calcd			
approx description[b]	symm	freq	int	obsvd freq	lit. freq
carbon dioxide	$D_{\infty h}$				ref 24
$\nu_a(CO_2)$	Σ_u	2376.3	675.8	2345.1	ca. 2340
				2343.6	
				2340.7	
$\beta(CO_2)$	$\prod_u$	667.1	30.3	674.0	ca. 668
				663.8	
				658.3	
				654.5	
carbon monoxide	$C_{\infty v}$				ref 27
$\nu_a(CO)$	Σ	2185.3	79.9		ca. 2138
ketene	C_{2v}				refs 25, 26
$\nu(=C=O)$	A_1	2188.7	678.5	2147.9	2142
				2144.8	
				2142.3	
				2141.4	
				2140.6	
				2138.7	
				2137.0	
				2134.6	
				2132.4	
oxiran-2-one	C_s				ref 31
$\nu(C=O)$	A'	1974.5	512.5	1954.5	ca. 1900
				1950.2	
				1946.1	
				1944.9	
				1942.0	
1,3-dioxolan-4-one	C_1				ref 33
$\nu(C=O)$	A	1850.4	393.0	1832.6	ca. 1780
				1817.4	
				1814.6	
$twist_a(CH_2)$	A	1208.6	233.6	1208.4	
$rock_a(CH_2)$	A	1198.6	66.2		
$twist_s(CH_2)$	A	1128.6	47.3	1128.0	
$wag_a(CH_2)$	A	1083.7	34.7	1086.5	
$rock_a(CH_2)$	A	1037.4	35.9	1034.4	
$\nu(CO)$	A	994.8	30.9	996.8	
$\nu(CO)$	A	951.5	105.7	964.3	
				961.4	
				958.0	
				957.2	
				955.3	
				953.9	
formaldehyde	C_{2v}				ref 35
$\nu_a(CH_2)$	B_2	2910.7	116.8	2870.0	2864.7
$\nu(C=O)$	A_1	1795.2	114.0	1738.0	1742.2
				1734.7	
				1733.5	
				1732.0	
oxirane	C_{2v}				ref 39
ring def.	A_1	878.8	71.7	903.3	877

[a] Photoproducts formed during irradiation of diglycolic anhydride (DGAn) in solid argon. Complete calculated spectra are presented in Tables S1−S7 (Supporting Information). [b] s = symmetric; a = antisymmetric; ν = stretching; β = in-plane bending; γ = out-of-plane bending; τ = torsion; scis = scissoring; rock = rocking; wag = wagging; twist = twisting.

tetrazolones contain three and four single bonds, respectively. In the previous studies of the UV-induced photochemistry of matrix-isolated tetrazoles and tetrazolones,[40] we have found that (i) there are multiple photochannels observed, with a pairwise cleavage of two formally single bonds in a particular reaction; (ii) if all the photochannels are considered, then each formally single bond is susceptible to photochemical cleavage; (iii) each single bond may be cleaved in combination with cleavage of some other single bond(s); different combinations result in different photochannels. Out of these combinations only those which result in radical species were not confirmed experimentally.[40] A similar situation occurs in DGAn. No experimental evidence of cleavage of pairs of bonds attached to the same oxygen atom (1,2) or (4,5) was observed (see Scheme 1 for explanation of bond numbering). Such cleavages would generate atomic oxygen radical. Similarly, no indications of photochannels involving cleavage of pairs of bonds attached to the same methylenic carbon (3,4) or (5,6) were found in the experimental spectra. The latter cleavages would lead to generation of methylene radical.

The photofragmentation of DGAn ring obeys certain regularities, and a mechanistic model accounting for these regularities is discussed below.

Analysis of the reactions presented in Scheme 1 reveals that photochannels a and b might be related. These two photochannels have a common photoproduct, carbon monoxide, which is formed by the cleavage of bonds 1 and 6. In channel a, the remaining molecular fragment rearranges to form a five-membered ring, whereas in channel b an additional bond is cleaved and the starting molecule splits into three pieces. The question arises whether in channel b the three bonds are cleaved simultaneously, in a concerted way, or the five-membered ring of 1,3-dioxolan-4-one formed in channel a undergoes the secondary photochemical reaction generating carbon dioxide and oxirane. Further questions also arise: if the cleavage of the DGAn ring in channel b is not concerted, may it proceed in another order, i.e., with the initial cleavage of different pairs of bonds, e.g., (3 and 6) or (1 and 3)? Does it also apply to other photochannels where more than two bonds must be cleaved to give the final set of photoproducts?

Scheme 2 represents a more detailed reaction scheme, where some possibilities of a stepwise ring cleavage are depicted. Let us consider channel c first. This channel results in the cleavage of bonds 1, 3, and 5 (see Scheme 2). The final result may be achieved via three different multistep channels. Namely cleavage of bond pairs (1,3), (1,5), and (3,5). If these possibilities were effective, then three additional reaction intermediates would be formed. These would correspond to γ-propiolactone (c1), acetic acid peroxy lactone (c2), and malonic anhydride (c3), respectively (see Scheme 2). However, these putative photoproducts were not observed in the experiment, which suggests that the photochemical cleavage of DGAn in channel c occurs in the concerted way, with simultaneous cleavage of three bonds.

Now, let us consider channel b, where bonds 1, 3, and 6 are cleaved (Scheme 1). The stepwise cleavage offers three possibilities: (1,3), (1,6), and (3,6). As it was shown before, the cleavage of the (1,6) type does occur in the experiment and corresponds to photochannel a. The cleavage of the (1,3) type would result in formation of carbon dioxide and γ-propiolactone, which is identical to channel c1 discussed just above. The different secondary cleavage of the 'might-be-formed' γ-propiolactone [structure c1 in Scheme 2] would then lead to the set of photoproducts characteristic of either channel b or channel c. Finally, the cleavage of the 3,6 type should lead to simultaneous formation of oxirane and oxalic anhydride [structure b1 in Scheme 2]. However, there is no experimental spectral evidence of formation of either γ-propiolactone or oxalic anhydride, and then it is very likely that the cleavage of the three bonds in photochannel b also occurs in a concerted way.

Let us also consider channel d. This photochemical channel leads to production of oxiran-2-one, which can subsequently

TABLE 5: Selected Natural Bond Orbitals (NBO) of Diglycolic Anhydride (DGAn) Obtained from the DFT(B3LYP)/aug-cc-pVTZ Calculations[a]

		coefficients		
bond orbital[b] T(A−B)	occupancy[c] (*e*)	%A	%B	description
σ(C1−C2)	1.99073	50.63	49.37	$0.7115sp^{(2.77)}d^{(0.01)} + 0.7026sp^{(1.67)}$
σ(C5−C4)				
σ(C1−O6)	1.98982	33.90	66.10	$0.5822sp^{(3.38)}d^{(0.01)} + 0.8130sp^{(2.64)}d^{(0.01)}$
σ(C5−O6)				
σ(C1−H10)	1.97230	61.44	38.56	$0.7838sp^{(2.88)}d^{(0.01)} + 0.6210s$
σ(C5−H9)				
σ(C1−H12)	1.97046	60.13	39.87	$0.7755sp^{(2.98)}d^{(0.01)} + 0.6314s$
σ(C5−H11)				
σ(C2−O3)	1.98812	31.39	68.61	$0.5603sp^{(2.75)}d^{(0.01)} + 0.8283sp^{(2.30)}d^{(0.01)}$
σ(C4−O3)				
σ(C2═O7)	1.99543	35.52	64.48	$0.5960sp^{(1.78)} + 0.8030sp^{(1.45)}d^{(0.02)}$
σ(C4═O8)				
π(C2═O7)	1.98922	32.07	67.93	$0.5663pd^{(0.02)} + 0.8242pd^{(0.04)}$
π(C4═O8)				
n_1(O3)	1.95483			$sp^{(1.53)}$
n_2(O3)	1.74417			$pd^{(0.02)}$
n_1(O6)	1.96410			$sp^{(1.20)}$
n_2(O6)	1.91757			p
n_1(O7)	1.98035			$sp^{(0.69)}$
n_1(O8)				
n_2(O7)	1.82823			$pd^{(0.21)}f^{(0.02)}$
n_2(O8)				
Ry_1*(C2)	0.01391			$sp^{(3.72)}d^{(0.04)}f^{(0.01)}$
Ry_1*(C4)				
σ*(C1−C2)	0.08317	49.37	50.63	$0.7026sp^{(2.77)}d^{(0.01)} - 0.7115sp^{(1.67)}$
σ*(C5−C4)				
σ*(C1−O6)	0.01833	66.10	33.90	$0.8130sp^{(3.38)}d^{(0.01)} - 0.5822sp^{(2.64)}d^{(0.01)}$
σ*(C5−O6)				
σ*(C1−H10)	0.01348	38.56	61.44	$0.6210sp^{(2.88)}d^{(0.01)} - 0.7838s$
σ*(C5−H9)				
σ*(C1−H12)	0.02717	39.87	60.13	$0.6314sp^{(2.98)}d^{(0.01)} - 0.7755s$
σ*(C5−H11)				
σ*(C2−O3)	0.12729	68.61	31.39	$0.8283sp^{(2.75)}d^{(0.01)} - 0.5603sp^{(2.30)}d^{(0.01)}$
σ*(C4−O3)				
σ*(C2═O7)	0.01395	64.48	35.52	$0.8030sp^{(1.78)} - sp^{(1.45)}d^{(0.02)}$
σ*(C4═O8)				
π*(C2═O7)	0.16438	67.93	32.07	$0.8242pd^{(0.02)} - 0.5663pd^{(0.04)}$
π*(C4═O8)				

[a] The presented description is made in the space of the input atomic orbitals [as given by the aug-cc-pVTZ basis set used in the calculations]. The %A and %B values correspond to the contributions of the atomic orbitals of the two atoms forming a bond (by order of appearance in the corresponding entry in the first column) for the NBO orbitals extracted from the polarization coefficients [(41)] given in the description of the NBO orbitals. [b] See atom numbering in Figure 1. [c] Occupancy is given with an exaggerated accuracy, as in the Gaussian output file.

TABLE 6: Stabilization Energies for the Selected Orbital Pairs as Given by the Second-Order Perturbation Theory Analysis of Fock Matrix in NBO Basis for Diglycolic Anhydride Obtained from the DFT(B3LYP)/aug-cc-pVTZ Calculations[a]

pair name	donor NBO	acceptor NBO	$E(2)^b$
A	n_2(O3)	π*(C2═O7)	36.13
B	n_2(O3)	π*(C4═O8)	36.13
C	n_1(O7)	Ry_1*(C2)	18.77
D	n_1(O8)	Ry_1*(C4)	18.77
E	n_2(O7)	σ*(C1−C2)	20.86
F	n_2(O8)	σ*(C5−C4)	20.86
G	n_2(O7)	σ*(C2−O3)	38.76
H	n_2(O8)	σ*(C4−O3)	38.76

[a] See atom numbering in Figure 1. [b] Energies in kcal mol^{-1}.

undergo secondary cleavage resulting in formation of carbon monoxide and formaldehyde. The latter two photoproducts were observed in the experiment, but they may result from alternative photochannels. The present experiments give no straight answer if this possibility is effective (or not). It is also possible that some branched reactions such as those presented in Scheme 2 contribute to the photochemistry of diglycolic anhydride.

Finally, it should be noted that all observed photochemical reaction channels involve the initial cleavage of one of the C−O bonds in the anhydride fragment (bonds 1 or 2), whereas almost all reaction channels involve also the cleavage of a C−C bond. These bonds are adjacent to the C═O fragments, which are the target of the initial UV excitation. In the next section, it will be shown that the strong orbital interactions between the C═O moieties and the adjacent C−O and C−C bonds make these latter more susceptible to the influence of the excitation (including, as observed, bond cleavage).

Natural Bond Orbitals (NBO) Analysis. NBO analysis provides an electronic structure description akin to the classic Lewis bonding theory.[41,42] Filled NBOs, empty bond NBOs, and non-Lewis extra valence Rydberg orbitals, as well as their interactions according to second-order perturbation theory of the Fock matrix,[41] are considered in this analysis. In the NBO analysis presented below, the calculated DFT(B3LYP)/aug-cc-pVTZ wave functions were considered.

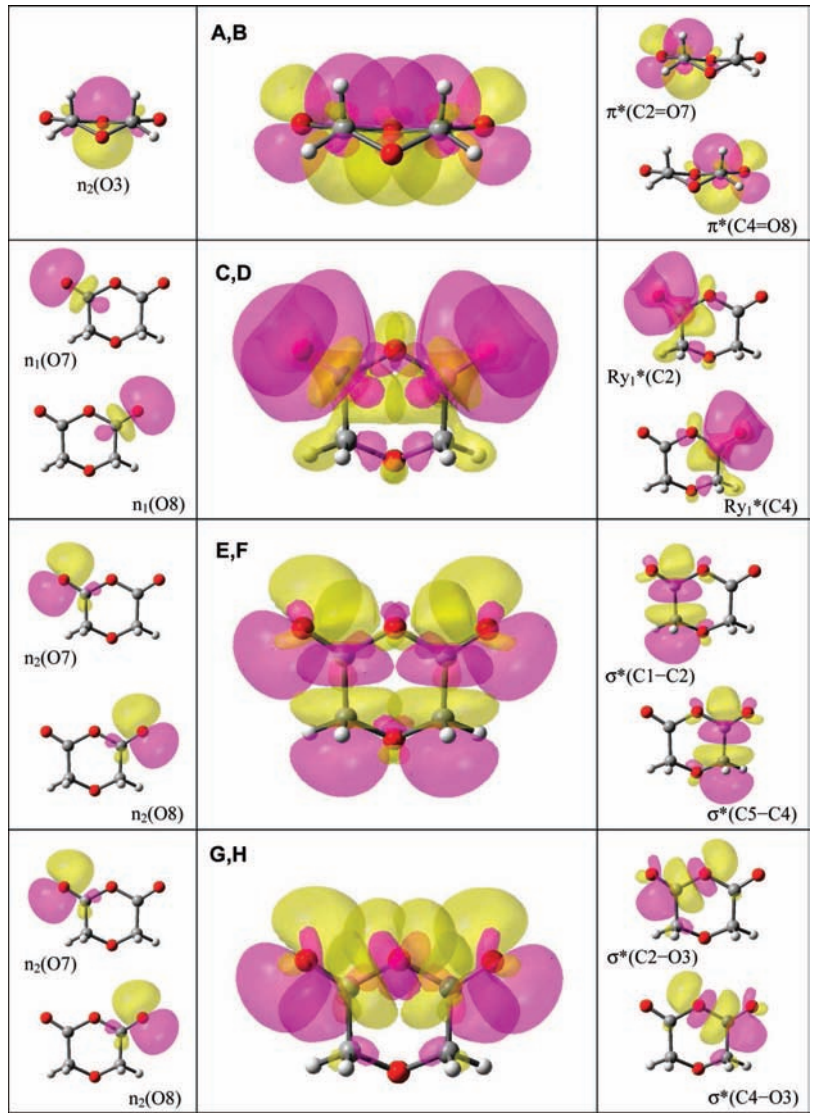

Figure 5. Electron density surfaces of selected preorthogonalized NBOs of diglycolic anhydride calculated at the DFT(B3LYP)/aug-cc-pVTZ level. Yellow and pink colors correspond to opposite signs. Isovalues of the electron densities are equal to 0.02 *e*. All donor NBOs are shown in the left column, whereas all acceptor NBOs are displayed in the right column. The middle column shows views of the donor and acceptor NBOs superimposed. Orbital interactions schemes shown in the middle column are named as A−H, as in Table 6. Color codes for atoms: red, oxygen; gray, carbon; white, hydrogen.

Selected NBOs, which were calculated to have a significant occupancy, are presented in Table 5. The description is made in the space of input atomic orbitals [as given by the aug-cc-pVTZ basis set used in the calculations]. The table also shows the percentage ratio of the atomic orbitals on each atom forming a bond, extracted from the polarization coefficients[41] of the NBO orbitals.

The NBO analysis reveals the following features: (i) The σ(C═O) bonding orbitals are, as expected, strongly polarized toward the oxygen atoms. (ii) The π(C═O) bonding orbitals are even more polarized toward the oxygen atoms, their occupancies being slightly smaller than those of the σ(C═O) orbitals (1.989 *e* vs 1.995 *e*). (iii) The σ^*(C═O) and π^*(C═O) antibonding orbitals are polarized toward the carbon atom, the second ones showing a larger occupancy than the first ones; the occupancy of the π^*(C═O) antibonding orbitals is as large as 0.164 *e*. (iv) The carbonyl carbon atoms are, as expected, hybridized sp^2, with the two hybrid orbitals forming the σ bond with the carbonyl oxygens and the adjacent carbon atoms having a larger s character and the one connecting the carbonyl carbon atom to the ring heteroatom having an increased p character. (v) The carbonyl oxygen atoms are hybridized sp; one of the two hybrid orbitals has a high p degree and forms the σ(C═O) bond, while the other has a high s content and is occupied by a lone pair of electrons; the two p orbitals form the π(C═O) bond and accommodate the second lone electron pair. (vi) The occupancy of the sp-hybrid lone-pair orbital of the carbonyl oxygens is relatively high (1.980 *e*), while that of the second lone-pair orbital is considerably low (1.828 *e*), indicating that the latter orbital is extensively involved in charge donation. (vii) Both ring oxygen atoms (O3 and O6) may be considered as hybridized sp^2, though the s and p contributions to the hybrid orbitals forming the two C−O bonds and that associated with the σ lone-electron pair are considerably different in the case of O6. Indeed, for this latter atom, the hybrid orbitals participating in the C−O bonds have a high p contribution, which make them look as sp^3 hybrids (that is why the C−O6−C angle is only 111.9°; see Table 1), while the hybrid orbital accommodating the σ lone-electron pair has a large s character, approaching that of an sp hybrid. Nevertheless, for both oxygen atoms, two hybrid orbitals are used to make the bonds with the neighboring carbon atoms and the third one accommodates one of the lone

electron pairs, whereas a pure p orbital accommodates the second lone electron pair (see Table 5). For both atoms, the occupancies of the p-type lone electron pair orbitals are smaller than those of the hybrid orbitals. However, it is the p-type lone electron pair of the anhydride oxygen atom (O3) the one that has the lowest occupancy among all occupied orbitals (1.744 *e*), which indicates that this orbital is a strong electron donor orbital, in line with its expected participation in the resonance interaction within the anhydride fragment. (viii) The hybrid orbitals involved in the ring C−O bonds exhibit a strong polarization toward the oxygen atoms and have an increased p character. In turn, the oxygen hybrid lone-electron pair orbitals have a reduced p character (see Table 5).

Table 6 shows the results of the second-order perturbation theory analysis of Fock matrix in NBO basis. This analysis is carried out by examining all possible stabilizing interactions between 'filled' (donor) Lewis-type NBOs and 'empty' (acceptor) non-Lewis NBOs and estimating their energetic importance by the second-order perturbation theory.[41] Since these interactions lead to donation of occupancy from the localized NBOs of the idealized Lewis structure into the empty non-Lewis orbitals (and thus, to departures from the idealized Lewis structure description), they are sometimes also referred to as 'delocalization' corrections to the zeroth-order natural Lewis structure. For each donor NBO (*i*) and acceptor NBO (*j*), the stabilization energy $E(2)$ associated with delocalization $i \rightarrow j$ is estimated as

$$E(2) = \Delta E_{ij} = q_i \frac{F(i,j)^2}{\varepsilon_j - \varepsilon_i} \quad (1)$$

where q_i is the donor orbital occupancy, ε_i and ε_j are diagonal elements (orbital energies) and $F(i, j)$ is the off-diagonal NBO Fock matrix element. In Table 6 only the most important interactions (corresponding to the largest $E(2)$ values) are presented. These interactions are also illustrated graphically in Figure 5.

The energetically most relevant orbital interactions are the following: (i) charge transfer from the p-type lone-electron pair of O3 to the π^*(C═O) bonds (Figure 5A,B), which is a measure of the delocalization within the O═C−O−C═O fragment; (ii) charge transfer from the in-plane p-type lone-electron pair of the carbonyl oxygens to the σ^*(C−C) and σ^*(C−O) antibonding orbitals (Figure 5E−H); these interactions correspond to the traditional back-donation effect from the carbonyl oxygen to the adjacent bonds, through the σ system; (iii) interactions between the sp-hybrid lone-electron pair orbital of the carbonyl oxygens and the carbonyl carbon atoms (through a Rydberg orbital) (Figure 5C,D), which also express a back-donation effect. It is interesting to note that similar orbital interactions have been recently found for the analogous five-ring heterocycle molecule, 2(5H)-furanone.[23]

Conclusions

The structure and photochemistry of diglycolic anhydride (DGAn; 1,4-dioxane-2,6-dione) isolated in a low-temperature argon matrix were studied by FTIR spectroscopy and DFT calculations. In the matrix, the DGAn molecule adopts an envelope conformation, closely resembling that found in the crystalline phase. Photochemical transformations induced by UV irradiation ($\lambda > 240$ nm) of the matrix-isolated compound were found to be complex, leading to formation of several photoproducts, which could be identified experimentally based on the comparison between the experimental spectra and those theoretically predicted by the DFT calculations. Four main photochemical channels could be identified and their relative efficiency estimated: (a) 1,3-dioxolan-4-one + CO (30%); (b) CO_2 + CO + oxirane (10%); (c) formaldehyde + ketene + CO_2 (10%), and (d) oxiran-2-one + oxiran-2-one (2%). The experiments also point to the occurrence of channels c and d through a concerted mechanism, involving cleavage of three bonds. The experimental observations evidence the occurrence of a number of secondary reactions. All observed photochemical processes involve cleavage of a C−O bond adjacent to a carbonyl group and also, in general, of one of the C−C bonds (which are also adjacent to the carbonyls), indicating a substantial degree of electronic coupling between the carbonyl groups and their adjacent bonds. This was fully confirmed by NBO analysis, which revealed that the most important NBO interactions were the charge transfer from the p-type lone-electron pair of O3 to the π^*(C═O) bonds (which is a measure of the π delocalization within the O═C−O−C═O fragment) and the charge transfer from the in-plane p-type lone-electron pair of the carbonyl oxygens to the adjacent σ^*(C−C) and σ^*(C−O) antibonding orbitals.

Acknowledgment. S.J. acknowledges the Portuguese Science Foundation (FCT) for a postdoctoral grant (SFRH/BPD/22410/2005).

Supporting Information Available: Tables S1−S7 are given as Supporting Information. This material is available free of charge via the Internet at http://pubs.acs.org.

References and Notes

(1) Jolivet, P.; Gans, P.; Triantaphylides, C. *Anal. Biochem.* **1985**, *147*, 86. Hewlett, T. P.; McMartin, K. E.; Lauro, A. J.; Ragan, F. A. *J. Toxicol.-Clin. Toxicol.* **1986**, *24*, 389. Petrarulo, M.; Marangella, M.; Linari, F. *Clin. Chim. Acta* **1991**, *196*, 17.

(2) Males, R. G.; Herring, F. G. *Biochim. Biophys. Acta-Biomembranes* **1999**, *1416*, 333. DiNardo, J. C.; Grove, G. L.; Moy, L. S. *Dermatol. Surg.* **1996**, *22*, 421. Perricone, N. V.; DiNardo, J. C. *Dermatol. Surg.* **1996**, *22*, 435. Moy, L. S. *Dermatol. Surg.* **1997**, *23*, 175. Moy, L. S.; Howe, K.; Moy, R. L. *Dermatol. Surg.* **1996**, *22*, 439. Moy, L. S.; Moy, R. L. *Dermatol. Surg.* **1996**, *22*, 419. Moy, L. S.; Murad, H.; Moy, R. L. *J. Dermatol. Surg. Oncol.* **1993**, *19*, 243. Newman, N.; Newman, A.; Moy, L. S.; Babapour, R.; Harris, A. G.; Moy, R. L. *Dermatol. Surg.* **1996**, *22*, 455. Rendon, M. I. *Cutis* **2007**, *79*, 3. Hundgeburth, A. *Hautarzt* **2007**, *58*, 800. Yener, G.; Baitokova, A. *Cosmet. Sci.* **2006**, *57*, 487. Katsambas, A. D. *Dermatology* **2005**, *210*, 39. Cook, K. K.; Cook, W. R. *Dermatol. Surg.* **2000**, *26*, 994. Dreno, B.; Katsambas, A.; Pelfini, C.; Plantier, D.; Jancovici, E.; Ribet, V.; Nocera, T.; Morinet, P.; Khammari, A. *Dermatology* **2007**, *214*, 260.

(3) Souza, S. R.; Vasconcellos, P. C.; Carvalho, L. R. F. *Atmos. Environ.* **1999**, *33*, 2563.

(4) Ervens, B.; Feingold, G.; Frost, G. J.; Kreidenweis, S. M. *J. Geophys. Res.-Atmos.* **2004**, *109*, D15205. Ervens, B.; Feingold, G.; Clegg, S. L.; Kreidenweis, S. M. *J. Geophys. Res.-Atmos.* **2004**, *109*, D15206. Havey, D. K.; Feierabend, K. J.; Vaida, V. *J. Phys. Chem. A* **2004**, *108*, 9069. Havey, D. K.; Vaida, V. *J. Mol. Spectrosc.* **2004**, *228*, 152.

(5) Reva, I. A.; Jarmelo, S.; Lapinski, L.; Fausto, R. *J. Phys. Chem. A* **2004**, *108*, 6982. Reva, I. D.; Jarmelo, S.; Lapinski, L.; Fausto, R. *Chem. Phys. Lett.* **2004**, *389*, 68.

(6) Kabir-ud-Din; Hartani, K.; Khan, Z. *Int. J. Chem. Kinet.* **2001**, *33*, 377. Kabir-ud-Din; Iqubal, S. M. S.; Khan, Z. *Colloid Polym. Sci.* **2005**, *284*, 276. Srivastava, A.; Behari, K. *J. Appl. Polym. Sci.* **2006**, *100*, 2480. Richardson, K.; Tolbert, N. E. *J. Biol. Chem.* **1961**, *236*, 1280.

(7) Torres, C.; Otero, C. *Enzyme Microb. Technol.* **1999**, *25*, 745.

(8) Chujo, K.; Kobayashi, H.; Suzuki, J.; Tokuhara, S.; Tanabe, M. *Makromol. Chem.* **1967**, *100*, 262.

(9) Takahashi, K.; Taniguchi, I.; Miyamoto, M.; Kimura, Y. *Polymer* **2000**, *41*, 8725.

(10) Gilding, D. K.; Reed, A. M. *Polymer* **1979**, *20*, 1459.

(11) Vinciguerra, V.; Bucci, R.; Marini, F.; Napoli, A. *J. Therm. Anal. Calorim.* **2006**, *83*, 475.

(12) Braslavsky, S.; Heicklen, J. *Chem. Rev.* **1977**, *77*, 473. Hiraoka, H. *J. Am. Chem. Soc.* **1973**, *95*, 1664. Krull, I. S.; Arnold, D. R. *Tetrahedron Lett.* **1969**, 4349.

(13) Chamberlain, G. A.; Whittle, E. *J. Chem. Soc. Faraday Trans. I* **1975**, *71*, 1978.

(14) Frisch, M. J.; Trucks, G. W.; Schlegel, H. B.; Scuseria, G. E.; Robb, M. A.; Cheeseman, J. R.; Montgomery, J. A., Jr.; Vreven, T.; Kudin, K. N.; Burant, J. C.; Millam, J. M.; Iyengar, S. S.; Tomasi, J.; Barone, V.; Mennucci, B.; Cossi, M.; Scalmani, G.; Rega, N.; Petersson, G. A.; Nakatsuji, H.; Hada, M.; Ehara, M.; Toyota, K.; Fukuda, R.; Hasegawa, J.; Ishida, M.; Nakajima, T.; Honda, Y.; Kitao, O.; Nakai, H.; Klene, M.; Li, X.; Knox, J. E.; Hratchian, H. P.; Cross, J. B.; Bakken, V.; Adamo, C.; Jaramillo, J.; Gomperts, R.; Stratmann, R. E.; Yazyev, O.; Austin, A. J.; Cammi, R.; Pomelli, C.; Ochterski, J. W.; Ayala, P. Y.; Morokuma, K.; Voth, G. A.; Salvador, P.; Dannenberg, J. J.; Zakrzewski, V. G.; Dapprich, S.; Daniels, A. D.; Strain, M. C.; Farkas, O.; Malick, D. K.; Rabuck, A. D.; Raghavachari, K.; Foresman, J. B.; Ortiz, J. V.; Cui, Q.; Baboul, A. G.; Clifford, S.; Cioslowski, J.; Stefanov, B. B.; Liu, G.; Liashenko, A.; Piskorz, P.; Komaromi, I.; Martin, R. L.; Fox, D. J.; Keith, T.; Al-Laham, M. A.; Peng, C. Y.; Nanayakkara, A.; Challacombe, M.; Gill, P. M. W.; Johnson, B.; Chen, W.; Wong, M. W.; Gonzalez, C.; Pople, J. A. Gaussian 03; Revision C.02 ed.; Gaussian, Inc.: Wallingford CT, 2004.

(15) Becke, A. D. *Phys. Rev. A* **1988**, *38*, 3098. Lee, C. T.; Yang, W. T.; Parr, R. G. *Phys. Rev. B* **1988**, *37*, 785.

(16) Kendall, R. A.; Dunning, T. H.; Harrison, R. J. *J. Chem. Phys.* **1992**, *96*, 6796.

(17) Schachtschneider, J. H.; Mortimer, F. S. Vibrational Analysis of Polyatomic Molecules. VI. FORTRAN IV Programs for Solving the Vibrational Secular Equation and for the Least-Squares Refinement of Force Constants; Project No. 31450, Structural Interpretation of Spectra; Shell Development Co., 1969.

(18) Le Fèvre, R. J. W.; Sundaram, A. *J. Chem. Soc.* **1962**, 4009.

(19) Bienko, D. C.; Michalska, D.; Roszak, S.; Wojciechowski, W.; Nowak, M. J.; Lapinski, L. *J. Phys. Chem. A* **1997**, *101*, 7834. Lapinski, L.; Nowak, M. J.; Bienko, D. C.; Michalska, D. *Phys. Chem. Chem. Phys.* **2002**, *4*, 1123.

(20) Brisse, F.; Sygusch, J. *Acta Crystallogr. Sect. B* **1975**, *31*, 2829.

(21) Levy, D. E.; Fügedi, P. *The Organic Chemistry of Sugars*; CRC/Taylor & Francis: Boca Raton, FL, 2006.

(22) Tamagawa, K.; Takemura, M.; Konaka, S.; Kimura, M. *J. Mol. Struct.* **1984**, *125*, 131. Blukis, U.; Myers, R. J.; Kasai, P. H. *J. Chem. Phys.* **1963**, *38*, 2753.

(23) Breda, S.; Reva, I.; Fausto, R. *J. Mol. Struct.* **2008**, *887*, 75.

(24) Dahoo, P. R.; Berrodier, I.; Raducu, V.; Teffo, J. L.; Chabbi, H.; Lakhlifi, A.; Abouaf-Marguin, L. *Eur. Phys. J. D* **1999**, *5*, 71.

(25) Zhang, X. K.; Parnis, J. M.; Lewars, E. G.; March, R. E. *Can. J. Chem.* **1997**, *75*, 276. McCluskey, M.; Frei, H. *J. Phys. Chem.* **1993**, *97*, 5204. Hochstrasser, R.; Wirz, J. *Angew. Chem. Int. Ed. Engl.* **1990**, *29*, 411. Moore, C. B.; Pimentel, G. C. *J. Chem. Phys.* **1963**, *38*, 2816. Romano, R. M.; Della Védova, C. O.; Downs, A. J. *J. Phys. Chem. A* **2002**, *106*, 7235.

(26) Reva, I. D.; Nowak, M. J.; Lapinski, L.; Fausto, R. *Chem. Phys. Lett.* **2006**, *429*, 382. Breda, S.; Reva, I.; Lapinski, L.; Fausto, R. *Phys. Chem. Chem. Phys.* **2004**, *6*, 929. Lapinski, L.; Nowak, M. J.; Les, A.; Adamowicz, L. *J. Am. Chem. Soc.* **1994**, *116*, 1461.

(27) Tso, T. L.; Lee, E. K. C. *J. Phys. Chem.* **1985**, *89*, 1618. Maier, G.; Reisenauer, H. P.; Egenolf, H. *Organometallics* **1999**, *18*, 2155. Dubost, H.; Abouaf-Marguin, L. *Chem. Phys. Lett.* **1972**, *17*, 269. Andrews, L.; Arlinghaus, R. T.; Johnson, G. L. *J. Chem. Phys.* **1983**, *78*, 6347. Loewenschuss, A.; Givan, A.; Nielsen, C. J. *J. Mol. Struct.* **1997**, *408*, 533.

(28) van Tilborg, W. J. M. *Tetrahedron Lett.* **1973**, *14*, 523.

(29) Maier, G.; Rohr, C. *Liebigs Ann.* **1996**, 307.

(30) Breda, S.; Reva, I.; Lapinski, L.; Fausto, R. *J. Phys. Chem. A* **2006**, *110*, 11034.

(31) Milligan, D. E.; Jacox, M. E. *J. Chem. Phys.* **1962**, *36*, 2911.

(32) Sander, W. W. *J. Org. Chem.* **1989**, *54*, 4265.

(33) Chapman, O. L.; Wojtkowski, P. W.; Adam, W.; Rodriguez, O.; Rucktäschel, R. *J. Am. Chem. Soc.* **1972**, *94*, 1365.

(34) Nyquist, R. A.; Fouchea, H. A.; Hoffman, G. A.; Hasha, D. L. *Appl. Spectrosc.* **1991**, *45*, 860.

(35) Bach, S. B. H.; Ault, B. S. *J. Phys. Chem.* **1984**, *88*, 3600. Diem, M.; Lee, E. K. C. *J. Phys. Chem.* **1982**, *86*, 4507. Lugez, C.; Schriver, A.; Schriver-Mazzuoli, L.; Lasson, E.; Nielsen, C. J. *J. Phys. Chem.* **1993**, *97*, 11617. Nelander, B. *J. Chem. Phys.* **1980**, *72*, 77. (d) Khoshkhoo, H.; Nixon, E. R. *Spectrochim. Acta, Part A* **1973**, *29*, 603.

(36) Breda, S.; Reva, I. D.; Lapinski, L.; Nowak, M. J.; Fausto, R. *J. Mol. Struct.* **2006**, *786*, 193.

(37) Reva, I. D.; Stepanian, S. G. *J. Mol. Struct.* **1995**, *349*, 337.

(38) Kus, N.; Breda, S.; Reva, I.; Tasal, E.; Ogretir, C.; Fausto, R. *Photochem. Photobiol.* **2007**, *83*, 1541. Kus, N.; Breda, S.; Reva, I.; Tasal, E.; Ogretir, C.; Fausto, R. *Photochem. Photobiol.* **2007**, *83*, 1237.

(39) Nakanaga, T. *J. Chem. Phys.* **1980**, *73*, 5451.

(40) Gómez-Zavaglia, A.; Reva, I. D.; Frija, L. M. T.; Cristiano, M. L. S.; Fausto, R. *Chem. Phys. Res. J.* **2008**, *1*, No. 4, article 2.

(41) Weinhold, F.; Landis, C. R. *Valency and Bonding: A Natural Bond Orbital Donor-Acceptor Perspective*; Cambridge University Press, New York, 2005.

(42) Foster, J. P.; Weinhold, F. *J. Am. Chem. Soc.* **1980**, *102*, 7211. Reed, A. E.; Curtiss, L. A.; Weinhold, F. *Chem. Rev.* **1988**, *88*, 899. Weinhold, F.; Landis, C. R. *Chem. Educ.: Res. Pract. Eur.* **2001**, *2*, 91.

JP805603B